Genetic Circuit-Host Ribosome Transactions: Diffusion-Reaction Model

Carlos Barajas and Domitilla Del Vecchio

Abstract— **Deterministic models of bacterial genetic circuits commonly assume a well-mixed ensemble of species. This assumption results in ordinary differential equations (ODEs) describing the rate of change of the mean species concentration. It is however well known that species are non-homogenously distributed within a bacterial cell, where genes on the chromosome are found mostly at the center of the cell while synthetic genes residing on plasmids are often found at the poles. Most importantly, ribosomes, the key gene expression resource, are also arranged according to a non-homogenous profile. Therefore, when analyzing the effects of sharing gene expression resources, such as ribosomes, among synthetic genetic circuits and chromosomal genes, it may be important to consider the effects of spatial heterogeneity of the relevant species. In this paper, we use a partial differential equation (PDE) model to capture the spatial heterogeneity of species concentration. Solutions to the model are gathered numerically and approximations are derived via perturbation analysis in the limit of fast diffusion. The solutions are compared to those of the conventional "well-mixed" ODE model. The fast-diffusion approximation predicts higher protein production rates for all mRNAs in the cell and in some cases, these rates are more sensitive to the activation of synthetic genes relative to the well-mixed model. This trend is confirmed numerically using common biological parameters to simulate the full PDE system.**

I. Introduction and Motivation

Synthetic genetic circuits are usually designed by assembling modules that have been previously characterized in isolation [1]. Because circuit modules all share the same limited resources required for gene expression, chiefly ribosomes, the composition of modules often creates unpredictable outcomes. In fact, when an input signal activates a synthetic circuit which demands resources, it depletes the resource pool and thus decreases the output of all other circuits in the network. This undesired cross-talk between circuits, prevents robust performance of modules and of the network in which these modules are embedded. In [2], it was shown that the expression levels of two synthetic genes with no direct coupling were constrained to an isocost line due to ribosome sharing. This cross-talk is not limited to local interactions; over-producing synthetic proteins decreases free ribosomes and thus lowers cellular growth rates [3].

It is desirable to use models that accurately capture ribosome sharing to gain insight into designing circuits within parameter ranges where cross-talk is minimal [4], as well as to guide the design of solutions that mitigate the effects of resource-sharing [5]. Current models, including the commonly used Ordinary Differential Equation (ODE) model, assume that all the species in the cell are well-mixed, and as such, do not capture any spatial heterogeneity. However, ribosomes tend to localize and therefore are not homogeneously distributed throughout the cell [6]. Furthermore, circuits tend to localize at the cells ends [7], away from the chromosome which is near mid-cell. These spatial features complicate ribosome transactions and raise doubt on whether the well-mixed model has sufficient fidelity to capture the effects of ribosome sharing on circuits behavior.

In this work, we propose a model of ribosome-sharing that captures the experimentally observed non-homogeneity of biomolecular species in the cell and investigate the coupling between the expression levels of otherwise unconnected genes. Specifically, we formulate a partial differential equation (PDE) model that captures the aforementioned spatial features and ribosome sharing to predict protein expression. The resulting nonlinear PDEs are solved numerically using a collocation method. Furthermore, an approximation is provided in the limit of fast diffusion.

In the limit of fast diffusion, the mRNA and ribosome spatial concentration profiles are not homogeneous due to the spatially varying available volume for the species to diffuse. For the fast-diffusion approximation, all mRNAs in the cell have a higher affinity to bind to ribosomes relative to the standard "well-mixed" ODE model. The increased affinity between mRNAs and ribosomes implies higher protein production rates for all mRNAs in the cell and, in some cases, these rates are more sensitive to the activation of synthetic genes. Similar trends were observed for the full PDE model relative to the well-mixed model via numerical simulations using common biological parameters.

This paper is organized as follows. In Sec. II, we derive the PDE model that we study in this paper. We consider the input to the system of PDEs to be the activation of a synthetic gene and the output to be the average concentration per cell of the expression level of all other genes. In Sec. III, matched asymptotic expansions are used to calculate an approximation of the PDE in the limit of fast diffusion. The implications of this approximation are provided in Sec. IV. In Sec. V an example with realistic biological parameters is provided. We end with conclusions and future work.

II. Ribosome Sharing Model

In this section, we derive a PDE model that captures the spatial distribution of genes (chromosome or plasmid), diffusion of species, and ribosome sharing among mRNAs. The resulting equations are then cast in dimensionless form. The inputs and outputs of the resulting system of PDEs are

This work was supported by AFOSR grant FA9550-14-1-006 . Carlos Barajas and Domitilla Del Vecchio are with the Department of Mechanical Engineering, MIT, Cambridge, MA 02139, USA carlobar@mit.edu (C. Barajas), ddv@mit.edu (D. Del Vecchio)

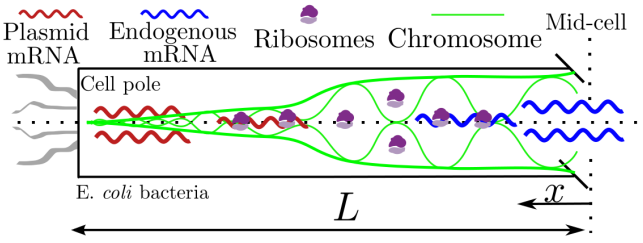

Fig. 1: Cylindrical cell geometry. The distance between the mid-cell and the poles is L. The horizontal dashed line denotes an axes of symmetry and the vertical dashed line denotes symmetry about the mid-cell. Plasmid genes are expressed at the cell poles. Endogenous cellular mRNAs are expressed along the chromosome (green line) whose density decreases away from mid-cell (increasing x). A higher chromosome density at a location x implies a lower available volume $v(x)$ for diffusion. mRNAs diffuse through the chromosome and compete for ribosomes.

specified and are used to determine how the activation of a synthetic gene affects the expression of other genes, on the chromosome or on plasmids. The well-mixed ODE model is then introduced for comparison with the PDE model.

A. Geometry and General Diffusion Model

The cell actively regulates its geometry to achieve a near-perfect cylindrical shape [8]. We model the cell as a cylinder of length (L). We assume angular and radial symmetry such that the concentration of a species varies only axially (the spatial x direction). Symmetry relative to the mid-cell is assumed and hence only half of the cell is considered. The geometry is shown in Fig. 1.

For any given biomolecular species in the cell S, conservation of the number of molecules leads to the one-dimensional balance equation (as derived in [9]):

$$\frac{\partial S(x,t)}{\partial t} = -\frac{1}{A(x)}\frac{\partial}{\partial x}[J(S,x)A(x)] + \sigma(S,x,t). \quad (1)$$

Here t denotes time, $S(x,t)$ is concentration per unit length, $A(x)$ is the cross-sectional area, $J(S,x)$ is the flux per unit area per unit time, and $\sigma(S,x,t)$ is a sink or source term (e.g., biochemical reactions). We define $v(x)$ to be the volume fraction (dimensionless) available to a species to diffuse within the chromosome (Fig. 1). The $v(x)$ depends on the local chromosome density at position x and the size of the species. An expression for the flux term, derived in [12] is:

$$J(S,x) = -D\left(\frac{\partial S(x,t)}{\partial x}v(x) - S(x,t)\frac{\partial v(x)}{\partial x}\right), \quad (2)$$

where D is the diffusion coefficient. The flux is driven by two mechanisms: the first is concentration gradients, which moves particles from high to low concentrations and the second drives particles to regions with a higher volume fraction. This second mechanism is refereed to as the excluded volume effects. From (2), if $|\frac{\partial S(x,t)}{\partial x}v(x)| < |S(x,t)\frac{\partial v(x)}{\partial x}|$ and $\frac{\partial S(x,t)}{\partial x}\frac{\partial v(x)}{\partial x} > 0$, then the net flux counterintuitively goes from low to high concentration. In Sec. IV, we show that the excluded volume effects are responsible for allowing inhomogeneous concentration gradients in the limit of fast diffusion. For this work, we assume a constant cross-sectional area along the axial direction. The boundary conditions (BC) are flux-free at the cell poles and at the cell center due to left-right symmetry:

$$J(S,0) = J(S,L) = 0. \quad (3)$$

Next, we specify the term $\sigma(S,x,t)$ in (1) by giving the biomolecular reactions that describe the sharing of ribosomes by endogenous and synthetic mRNA species.

B. Diffusion in a Ribosome Sharing Context

Suppose the cell contains $N = N_1 + N_2$ mRNA species (N_1 endogenous and N_2 synthetic) denoted as $m_i(x,t)$ for $i = 1,2,\ldots,N$, each binding to free ribosomes $R(x,t)$ to form an mRNA-ribosome complex $c_i(x,t)$, which is converted to protein $P_i(x,t)$ through the translation process [10]. The corresponding biochemical reactions are [11]

$$\emptyset \xrightarrow{\alpha_i} \mathrm{m_i},\ \emptyset \xrightarrow{\alpha_r} \mathrm{R},\ \mathrm{m_i} \xrightarrow{\gamma+\mu} \emptyset,\ \mathrm{c_i} \xrightarrow{\mu} \emptyset,\ \mathrm{R} \xrightarrow{\mu} \emptyset,$$
$$\mathrm{m_i} + \mathrm{R} \underset{\mathrm{d_i}}{\overset{\mathrm{a_i}}{\rightleftharpoons}} \mathrm{c_i} \xrightarrow{\kappa_i} \mathrm{P_i} + \mathrm{m_i} + \mathrm{R},\ \mathrm{c_i} \xrightarrow{\gamma} \mathrm{R}, \quad (4)$$

where γ is the rate of mRNA degradation; μ is the dilution constant due to growth rate; a_i and d_i are the association and dissociation constants, respectively, of mRNA-ribosome binding; and κ_i is the rate at which proteins are synthesized. The transcription profile $\alpha_i = \alpha_i(x,t)$ determines whether $m_i(x,t)$ is transcribed from endogenous or synthetic genes. We use D to denote the average diffusion coefficient of the mRNA-ribosome complex's, which includes free mRNAs as done in [12]. Similarly D_r denotes the free-ribosome diffusion coefficient. The available volumes for mRNA, mRNA-ribosome complex, and free ribosomes are: v_m, v_c, and v_r, respectively.

We lump all endogenous genes into one equivalent gene ($N_1 = 1$) and assume that their mRNAs are synthesized at a constant temporal rate with a spatial profile given by: $\alpha_e(x) = \alpha_{e,l}\rho(x)$, where $\rho(x) = \frac{1}{1+e^{20(x/L-1/2)}}$, is the normalized local DNA density in the cell, empirically calculated in [12]. The constant $\alpha_{e,l}$, is chosen such that the total transcription in the cell $\bar{\alpha}_e = 2\int_0^L \alpha_e(x)dx$. The production of ribosomes is given by: $\alpha_r(x) = \alpha_{r,l}\rho(x)$, such that $2\int_0^L \alpha_r(x)dx = \bar{\alpha}_r$ for some specified cumulative ribosome production $\bar{\alpha}_r$ in the cell. For synthetic DNA expressed from a plasmid, the mRNA transcription profile $\alpha_i(x)$ is concentrated near the cell poles ($x = L$) [13], such that $2\int_0^L \alpha_i(x)dx = \bar{\alpha}_i$, to achieve a total production $\bar{\alpha}_i$ of that synthetic mRNA per cell. The localization of endogenous DNA mid-cell and of plasmid DNA in the cell poles is illustrated in Fig. 1.

We work with variables and parameters in their dimensionless form to identify the underlying time and length scales that govern the physics of the model. We nondimensionalize the system variables using the mRNA degradation (γ) as the characteristic time scale, the endogenous mRNA per length ($\frac{\alpha_{e,l}}{\gamma}$) as the characteristic concentration per length scale, and the length of the cell (L) as the characteristic length:

$t^* = t\gamma,\ y^* = y\frac{\gamma}{\alpha_{e,l}},\ x^* = \frac{x}{L}$, where y denotes some general concentration per unit length and the superscript of $*$ is used on the dimensionless variable. All concentrations are related to the endogenous mRNA production because it is typically known. The dimensionless mRNA and complex dynamics for $i = 1, 2, \ldots, N$ are given by:

$$\frac{\partial m_i^*}{\partial t^*} = \chi_m\left(\frac{\partial^2 m_i^*}{\partial x^{*2}}v_m - m_i^*\frac{\partial^2 v_m}{\partial x^{*2}}\right) + \alpha_i^* + K_i c_i^* - 2\theta_i R^* m_i^* - (1+\mu^*)m_i^*, \quad (5a)$$

$$\frac{\partial c_i^*}{\partial t^*} = \chi_m\left(\frac{\partial^2 c_i^*}{\partial x^{*2}}v_c - c_i^*\frac{\partial^2 v_c}{\partial x^{*2}}\right) + 2\theta_i R^* m_i^* - (1+K_i+\mu^*)c_i^*, \quad (5b)$$

where $\alpha_i^* = \frac{\alpha_i}{\alpha_{e,l}}$, $K_i = \frac{\kappa_i + d_i}{\gamma}$ and $2\theta_i = \frac{a_i \alpha_{e,l}}{\gamma^2}$, $\chi_m = \frac{D}{L^2\gamma}$, $\mu^* = \frac{\mu}{\gamma}$, and $x^* \in [0,1]$. The ribosome dynamics are:

$$\frac{\partial R^*}{\partial t^*} = \chi_r\left(\frac{\partial^2 R^*}{\partial x^{*2}}v_r - R^*\frac{\partial^2 v_r}{\partial x^{*2}}\right) + \sum_{i=1}^{N}\left((K_i+1)c_i^* - 2\theta_i R^* m_i^*\right) + \alpha_r^*\rho - \mu^* R^*, \quad (5c)$$

where $\chi_r = \frac{D_r}{L^2\gamma}$ and $\alpha_r^* = \frac{\alpha_{r,l}}{\alpha_{e,l}}$. The boundary conditions remain flux-free as in (3) for all species. A quantity of interest is the mean mRNA-ribosome complex given by:

$$\overline{c}_i^*(t^*) = 2\int_0^1 c_i^*(x^*, t^*)dx^*, \quad (5d)$$

which we therefore view as the output of the system of PDEs given in equations (5a)-(5c). The factor two accounts for the other symmetric half of the cell. We are interested in $\overline{c}_i^*(t^*)$ because it serves as a proxy for gene expression. The production rate of protein $\overline{P}_i^*$ is given by $\kappa_i\overline{c}_i^*$ and it is the quantity sensitive to fluctuations in ribosome concentration. The output is taken in terms of concentrations per cell for comparability with the commonly used ordinary differential equation (ODE) model, which assumes that the contents in the cell to be spatially homogeneous (referred to as "well-mixed" [14]). Furthermore, concentrations per cell are often the variables measured experimentally [15].

For the remainder of this paper, we proceed with the assumption that all variables are in their dimensionless form and hence, for ease of notation drop the $*$ superscript.

C. Inputs and Outputs

To quantify the extent to which the activation of a synthetic gene affects the mean expression of other genes ($\overline{c}_i$ in (5d)), we let the input of system (5) be mRNA production rate $\alpha_i(x,t)$, for some i. For a variable $y(x,t)$, the per cell concentration is denoted using an overbar and it is given by: $\overline{y}(t) = 2\int_0^1 y(x,t)dx$. Therefore, the spatially averaged dynamics of (5) are given by:

$$\frac{d\overline{m}_i}{dt} = \bar{\alpha}_i + K_i\overline{c}_i - (1+\mu)\overline{m}_i - \theta_i f_i(t)\overline{m}_i\overline{R}, \quad (6a)$$

$$\frac{d\overline{c}_i}{dt} = -(1+K_i+\mu)\overline{c}_i + \theta_i f_i(t)\overline{m}_i\overline{R}, \quad (6b)$$

$$\frac{d\overline{R}}{dt} = \bar{\alpha}_r - \mu\overline{R} + \sum_{i=1}^{N}\left((1+K_i)\overline{c}_i - \theta_i f_i(t)\overline{m}_i\overline{R}\right), \quad (6c)$$

where

$$f_i(t) = \frac{\int_0^1 m_i(x,t)R(x,t)dx}{\int_0^1 m_i(x,t)dx\int_0^1 R(x,t)dx}. \quad (7)$$

Even though (6) is written in terms of ODEs, to calculate $\overline{c}_i$, the PDEs must be solved because (7) depends on the PDE variables $m_i(x,t), \forall i$ and $R(x,t)$. However, in Sec. IV, we show that in the limit of fast diffusion, (7) depends solely on the available volume profiles and hence the PDEs can be bypassed. For comparison, we define the well-mixed model.

Definition 1: The well-mixed ODE model is given by setting $f_i(t) = 1,\ \forall t \in [0,\infty), \forall i$ in (6) and (7).

The term (7) can be interpreted as a modification to θ_i which is a measure of the affinity between the mRNA and ribosome. Hence, f_i provides a measure to compare how close the average concentrations predicted by the PDE model are to those of the "well-mixed" ODE model.

Lemma 1: Suppose that at some fixed t, $m_i(x,t)$ and $R(x,t)$ (as in (7)) are both strictly monotone in x. If $\frac{\partial R}{\partial x}\frac{\partial m}{\partial x} > 0$, then $f_i > 1$. If $\frac{\partial R}{\partial x}\frac{\partial m}{\partial x} < 0$, then $f_i < 1$. Equality holds ($f_i = 1$) if and only if either $m(x,t)$ or $R(x,t)$ are constant in x.

Proof: This follows from applying the Chebyshev Integral Inequality [16] to (7). ■

Thus, if $f_i > 1$, it implies that m_i has a higher affinity to ribosomes relative to the well-mixed model.

III. Analysis: Limit of Fast Diffusion

For a given species with diffusion coefficient D, the time scale associated with diffusion is given by $\tau_D = \frac{D}{L^2}$. In *E. coli*, diffusion is fast due to its small length ($L = 1.5\mu$m). The diffusion time of a protein across the cell is about 0.01 seconds, which is fast compared to the cell doubling time (greater than 20 minutes) and mRNA degradation, which is about 3 minutes [17]. In what follows, we use matched asymptotic expansions in time to derive an approximation for (5) in the limit of fast diffusion [18]. If the available volume fraction term in (2) were spatially constant, then the results in [19] could be directly applied. However, due to the space varying available volume fraction term in (2), this approximation cannot be readily derived. Thus, in the following section we provide the mathematical machinery needed to derive a fast-diffusion approximation to (5).

A. Preliminaries

Notation: Let $\boldsymbol{z} = [z_1, \ldots, z_n]^T \in \mathbb{R}^n$ and the j-th component of $\boldsymbol{z}$ is denoted as $\boldsymbol{z}^j$. A vector of zeros is denoted as $\mathbf{0}_n = [0, \ldots, 0]^T \in \mathbb{R}^n$ and we use $\boldsymbol{A} = \text{diag}(\boldsymbol{v}) \in \mathbb{R}^{n\times n}$ to refer to a matrix with all zeros in the off-diagonals and diagonal elements specified by the vector $\boldsymbol{v}$. The (j,k)-th element of $\boldsymbol{A}$ is denoted by $\boldsymbol{A}^{j,k}$ and $\boldsymbol{I}_{n,n}$ is the identity matrix in $\mathbb{R}^n$. $\mathbb{R}^n_+$ denotes the positive orthant of $\mathbb{R}^n$. Let $\Omega = (0,1)$, $\overline{\Omega} = [0,1]$, $\partial\Omega = \{0,1\}$

Definition 2: (Weighted L^2 space) For a continuous function $v(x) : \overline{\Omega} \to \mathbb{R}_+$ we denote $L^2_v(\Omega)$ as a weighted space of the square integrable functions such that $f \in$

$L^2_v(\Omega)$ if and only if $f\sqrt{v(x)} \in L^2(\Omega)$. The inner-product is defined as $(f,g)_v := \int_\Omega f(x)\bar{g}(x)v(x)$, for $f, g \in L^2_v$.

Definition 3: (Linear Differential Operator: $\mathcal{L}_v$) For a continuously differentiable function $v(x) : \overline{\Omega} \to \mathbb{R}_+$, we define the operator $\mathcal{L}_v : L^2_v(\Omega) \to L^2_v(\Omega)$, where $\mathcal{L}_v(y) := -\frac{1}{v(x)}\frac{\partial}{\partial x}\big(v(x)^2\frac{\partial}{\partial x}(y)\big)$, with domain $D(\mathcal{L}_v) = \{y \in L^2_v(\Omega) : y \text{ and } \frac{\partial y}{\partial x} \text{ are absolutely continuous, } \mathcal{L}_v(y) \in L^2_v(\Omega), \text{ and } \frac{\partial y}{\partial x}\big|_{\partial\Omega} = 0\}$.

Lemma 2: (Positive semidefinite and self-adjoint Operator) The operator $\mathcal{L}_v$ in Definition 3:

I Has countably many, real, and distinct eigenvalues such that $\lambda_0 < \ldots < \lambda_n < \ldots$ and $\lambda_n \to \infty$ as $n \to \infty$

II The set of corresponding eigenfunctions $\{\psi_i(x)\}$ forms an orthonormal basis for $L^2_v(\Omega)$

III $\lambda_0 = 0$ and $\psi_0 = (\int_\Omega v)^{-1/2}$.

Proof: The proof of (I) and (II) follow from Sturm-Liouville theory [20]. To prove (III), notice $\mathcal{L}_v\psi_i = \lambda_i\psi_i$ and taking the inner product of both sides with ψ_i, using orthonormality, and integrating by parts:

$$\lambda_i = (L\psi_i, \psi_i)_v = \int_\Omega \Big(-\frac{\partial}{\partial x}\Big(v^2\frac{\partial}{\partial x}\psi_i\Big)\Big)\psi_i$$
$$= \underbrace{-\psi_i v^2 \frac{\partial \psi_i}{\partial x}\Big|_{\partial\Omega}}_{0} + \int_\Omega \left(v\frac{\partial\psi_i}{\partial x}\right)^2 \geq 0. \quad (8)$$

The minimum of (8) is achieved ($\lambda_0 = 0$) for $\psi_0 = (\int_\Omega v)^{-1/2}$, since $\mathcal{L}_v(\psi_0) = 0$ and $||\psi_0||_{L^2_v} = \sqrt{(\psi_0,\psi_0)_v} = 1$ and therefore $\lambda_i > 0, \forall i > 0$. ■

Next, we introduce a general system and approximate its solution in the limit of a parameter approaching zero. In Sec. IV, after a change of coordinates, we apply the results of the analysis to (5) in the limit of fast diffusion.

For $\boldsymbol{z} \in \mathbb{R}^n$ and to each $\boldsymbol{z}^j$ we attach a $v_j(x) : \overline{\Omega} \to (0,1]$ which is twice continuously differentiable. Consider the system:

$$\frac{\partial \boldsymbol{z}(x,t)}{\partial t} = \boldsymbol{A}\boldsymbol{\mathcal{L}}(x,\boldsymbol{z}) + \boldsymbol{F}(x,\boldsymbol{z}),\ t > 0, x \in \Omega, \quad (9a)$$
$$\frac{\partial \boldsymbol{z}(x,t)}{\partial x} = \boldsymbol{0}_N, \quad t > 0, x \in \partial\Omega, \quad (9b)$$
$$\boldsymbol{z}(x,0) = \boldsymbol{z}_{00}(x), \quad x \in \Omega, \quad (9c)$$

where $\boldsymbol{A} = \text{diag}([\chi_1, \ldots, \chi_n]^T)$ for $\chi_i \in \mathbb{R}_+$, $\boldsymbol{\mathcal{L}} : \Omega \times \mathbb{R}^n \to \mathbb{R}^n$ such that $\boldsymbol{\mathcal{L}}^j = -\mathcal{L}_{v_j}(\boldsymbol{z}^j)$ as in Definition 3, $\boldsymbol{F} : \overline{\Omega} \times \mathbb{R}^n \to \mathbb{R}^n$, and $\boldsymbol{z}_{00} : \overline{\Omega} \to \mathbb{R}^n$ and $\boldsymbol{z}^j_{00} \in L^2_{v_j}(\Omega)$. It is assumed that $\boldsymbol{F}$ is twice continuously differentiable in both of its arguments and $\boldsymbol{F}_i \geq 0$ when $x \in \overline{\Omega}$ and $\boldsymbol{z}^i = 0$. These assumptions guarantee well-posedness of (9) [21].

B. Approximate solution through Matched Asymptotic Expansions

Let $\boldsymbol{A} = \frac{1}{\epsilon}I_{n,n}$ with $0 < \epsilon \ll 1$ such that (9a) becomes:

$$\epsilon\frac{\partial \boldsymbol{z}}{\partial t} = \boldsymbol{\mathcal{L}}(x,\boldsymbol{z}) + \epsilon\boldsymbol{F}(x,\boldsymbol{z}), \quad (10)$$

subject to (9b) and (9c). To obtain an approximate solution to (10) as $\epsilon \to 0^+$, we use the Method of Matched Asymptotic Expansions [18], which is often used for singularly perturbed systems (see [19], for example). The following preliminary claim is needed to carry out the expansion.

Claim 1: For a continuously differentiable function $v(x) : \overline{\Omega} \to \mathbb{R}_+$ and some $y_{00}(x) \in L^2_v(\Omega)$, the solution to:

$$\frac{\partial y(x,t)}{\partial t} + \mathcal{L}_v(y) = 0 \quad t > 0, x \in \Omega \quad (11)$$
$$y(x,0) = y_{00}(x), \quad x \in \Omega, \quad (12)$$

is given by $y = \frac{\int_\Omega y_{00}(x)v(x)}{\int_\Omega v(x)} + \mathcal{O}(e^{-\delta t})$ for some $\delta > 0$.

Proof: Assume the solution is in the form $y(x,t) = \psi(x)Y(t)$ and thus

$$\frac{\frac{\partial}{\partial t}Y(t)}{Y(t)} = -\mathcal{L}_v(\psi(x))/\psi(x) = -\lambda \implies Y(t) = \alpha e^{-\lambda t}.$$

notice that λ is an eigenvalue of $\mathcal{L}_v$ and $\psi(x)$ is the associated eigenfunction. Thus from Lemma 2, the solution can be written as $y(x,t) = \alpha_0(\int_\Omega v(x))^{-1/2} + \sum_{i=1}^\infty \alpha_i\psi_i(x)e^{-\lambda_i t}$ where $\lambda_i > 0, \forall i > 0$. Since $\{\psi_i\}$ forms an orthonormal basis of $L^2_v(\Omega)$, the initial conditions are satisfied and any other solution can be written in terms of $\{\psi_i\}$, justifying the separation of variables. Notice $y_{00}(x) = \sum_{i=0}^\infty \alpha_i\psi_i$ and by orthogonality $(y_{00},\psi_0)_v = (\alpha_0\psi_0,\psi_0)_v = \alpha_0$ and thus $\alpha_0 = (y_{00},\psi_0)_v$. Here $\delta = \lambda_1 > 0$. ■

Theorem 1: An approximate solution to (10) subject to (9b) and (9c) as $\epsilon \to 0^+$, is given by:

$$\boldsymbol{z}^j(x,t) = \beta_j(t) + \mathcal{O}(e^{-\delta_j t/\epsilon}) + \mathcal{O}(\epsilon), \quad (13a)$$

where $\delta_j > 0$ and $\beta_j(t)$ satisfies:

$$\frac{d\beta_j(t)}{dt} = \frac{\int_\Omega \boldsymbol{F}^j(x,\boldsymbol{\beta})v_j(x)}{\int_\Omega v_j(x)};\ \beta_j(0) = \frac{\int_\Omega \boldsymbol{z}^j_{00}(x)v_j(x)}{\int_\Omega v_j(x)}, \quad (13b)$$

where $\boldsymbol{\beta} = [\beta_1, \ldots, \beta_n]^T$.

Proof: To study the fast dynamics of (10), we introduce the fast time scale $\tau = t/\epsilon$ and the inner solution of (10) $\boldsymbol{z}_{\text{in}}(\tau,x,\epsilon)$, which is required to satisfy:

$$\frac{\partial \boldsymbol{z}_{\text{in}}}{\partial \tau} = \boldsymbol{\mathcal{L}}(x,\boldsymbol{z}_{\text{in}}) + \epsilon\boldsymbol{F}(x,\boldsymbol{z}_{\text{in}}), \quad (14)$$

with the initial and boundary conditions given in (9b)-(9c). Assume the asymptotic expansion of $\boldsymbol{z}_{\text{in}}$ in terms of ϵ:

$$\boldsymbol{z}_{\text{in}}(x,\tau,\epsilon) = \sum_{i=0}^\infty \epsilon^i \boldsymbol{u}_i(x,\tau), \quad \epsilon \to 0^+, \quad (15)$$

where each $\boldsymbol{u}_i$ satisfies the boundary conditions in (9b) and

$$\boldsymbol{u}_0(x,0) = \boldsymbol{z}_{00}(x),\ \boldsymbol{u}_i(x,0) = \boldsymbol{0}_n, \forall i > 0.$$

Substituting (15) into (14) and collecting the $\mathcal{O}(1)$ terms, we obtain:

$$\frac{\partial \boldsymbol{u}_0(x,\tau)}{\partial \tau} = \boldsymbol{\mathcal{L}}(x,\boldsymbol{u}_0). \quad (16)$$

The solution to (16) is given by Claim 1 and thus:

$$\boldsymbol{z}^j_{\text{in}} = \boldsymbol{u}^j_0 + \mathcal{O}(\epsilon) = \frac{\int_\Omega \boldsymbol{z}^j_{00}v_j(x)}{\int_\Omega v_j(x)} + \mathcal{O}(e^{-\delta_j t/\epsilon}) + \mathcal{O}(\epsilon).$$

To determine the dynamics governed by the slow time scale t, we introduce the outer solution $\boldsymbol{z}_{\text{out}}(x,t,\epsilon)$, and require it to satisfy

$$\epsilon\frac{\partial \boldsymbol{z}_{\text{out}}}{\partial t} = \boldsymbol{\mathcal{L}}(x,\boldsymbol{z}_{\text{out}}) + \epsilon\boldsymbol{F}(x,\boldsymbol{z}_{\text{out}}),$$

along with the boundary conditions in (9b). Rather than satisfying the initial conditions (9c), we require $\boldsymbol{z}_{\text{out}}(x,t\to 0,\epsilon) = \boldsymbol{z}_{\text{in}}(x,\tau\to\infty,\epsilon)$. We assume the following asymptotic expansion of $\boldsymbol{z}_{\text{out}}$ in terms of ϵ:

$$\boldsymbol{z}_{\text{out}}(x,t,\epsilon) = \sum_{i=0}^{\infty}\epsilon^i\hat{\boldsymbol{u}}_i(x,t), \quad \epsilon\to 0^+, \tag{17}$$

where each $\hat{\boldsymbol{u}}_i$ satisfies (9b). Substituting (17) into (10), yields:

$$0 = \boldsymbol{\mathcal{L}}(x,\hat{\boldsymbol{u}}_0), \tag{18}$$

$$\frac{\partial\hat{\boldsymbol{u}}_0}{\partial t} - \boldsymbol{F}(x,\hat{\boldsymbol{u}}_0) = \boldsymbol{\mathcal{L}}(x,\hat{\boldsymbol{u}}_1), \tag{19}$$

where (18) and (19) were obtained by collecting the $\mathcal{O}(1)$ and $\mathcal{O}(\epsilon)$ terms, respectively. From (18), $\hat{\boldsymbol{u}}_0^j = \beta_j(t)$, for some undetermined $\beta_j(t)\in\mathbb{R}$. From the boundary conditions (9b): $(\mathcal{L}_{v_j}(\hat{\boldsymbol{u}}_1^j),1)_{v_j} = 0$, thus $\int_\Omega\left[(\frac{\partial\hat{\boldsymbol{u}}_0^j}{\partial t} - \boldsymbol{F}^j(x,\hat{\boldsymbol{u}}_0))v_j(x)\right] = 0$. Hence, $\beta_j(t)$ is constrained as shown in (13b). Finally, $\boldsymbol{z}^j = \boldsymbol{z}_{\text{in}}^j + \boldsymbol{z}_{\text{out}}^j - \frac{\int_\Omega \boldsymbol{z}_{00}^j v_j(x)}{\int_\Omega v_j(x)}$ as in (13a). ■

Remark 1: For $\boldsymbol{z}^j$ as in (13), we define $\boldsymbol{w}^j(x,t) = v_j(x)\boldsymbol{z}^j(x,t)$, then $\overline{\boldsymbol{w}}^j = \int_\Omega \boldsymbol{w}^j = (\boldsymbol{z}^j,1)_{v_j}$ and by the orthogonality of the eigenfunctions: $\overline{\boldsymbol{w}}^j(t) = \beta_j(t)\int_\Omega v_j(x) + \mathcal{O}(\epsilon), \forall t\geq 0$. Thus, the spatially averaged solution $\overline{\boldsymbol{w}}^j(x)$, only depends on the zeroth eigenvalue of $\mathcal{L}_{v_j}$.

IV. Implications to Resource Sharing

Next, we apply the theoretical findings from Sec. III to the PDE system (5) after a change of coordinates and obtain an approximate solution in the limit of fast diffusion. We discuss the implications of the approximation in the context of ribosome sharing and compare to the well-mixed model.

A. Approximate Solution

Claim 2: Let $\boldsymbol{y} = [R, m_1,\dots,m_N,c_1,\dots,c_N]^T$ be the species corresponding (5) and $M = 2N+1$. For each species $\boldsymbol{y}^j$ we let $v_j(x):\bar{\Omega}\to(0,1]$ be the associated available volume profile. Assume $v_j(x)$ and $\alpha_j(x)$ are sufficiently smooth $\forall j$ and $\chi_m = \chi_r = \chi = \frac{1}{\epsilon}$, then as $\epsilon\to 0^+$:

$$\boldsymbol{y}^j = v_j(x)\left(\frac{\overline{\boldsymbol{w}}^j(t)}{\int_\Omega v_j} + \mathcal{O}(e^{-\delta_j t/\epsilon}) + \mathcal{O}(\epsilon)\right), \tag{20a}$$

where $\delta_j > 0$ and $\overline{\boldsymbol{w}}(t) = [\overline{R},\overline{m}_1,\dots,\overline{m}_N,\bar{c}_1,\dots,\bar{c}_N]^T$ is the solution of (6) with (7) given by

$$f_j = f = \frac{\int_\Omega v_r v_m}{\int_\Omega v_r\int_\Omega v_m},\ \forall j. \tag{20b}$$

The spatial averaged solution is given by,

$$\overline{\boldsymbol{y}}(t) = \int_\Omega \boldsymbol{y}(x,t) = \overline{\boldsymbol{w}}(t) + \mathcal{O}(\epsilon). \tag{20c}$$

Proof: Denoting $\boldsymbol{z}\in\mathbb{R}^M$ such that $\boldsymbol{z}^j = \boldsymbol{y}^j/v_j$, then the $\boldsymbol{z}$ dynamics are in the form given by (9) where $\boldsymbol{z}_{00}^j = \boldsymbol{y}^j(x,0)/v_j(x)$ and $\boldsymbol{A} = \chi I_{N,N}$. Thus, applying Theorem 1 we arrive at (20) and (20b). Finally, (20c) follows from the discussion in Remark 1. ■

Thus, in the limit of fast diffusion, any initial spatial distribution $\boldsymbol{y}^j(x,0)$ will converge to a spatial profile mirroring the available volume profile $v_j(x)$ (not homogenize) on a fast time scale associated with diffusion. The spatial average value per cell $\int_\Omega \boldsymbol{y}^j(x,0)$ is conserved during this fast transient. Thereon, the reaction dynamics take place on this spatial manifold. Since concentrations per cell are given by (20c), it implies that to compute the output (5d) in this limiting case, one can bypass solving the PDEs in (5). Rather, one solves the ODE model (6) with (7) given by (20b).

B. Implications of Approximate Solution

If (7) is given by $f_i = f, \forall i$, then: when $f = 1$, (6) coincides with the well-mixed model and when f is given by (20b), (6) coincides with the fast-diffusion approximation. We now determine how these different values of f affect the output of interest $\bar{c}_i$ (5d). For these two cases f can be treated as a system parameter.

First, we bound (20b). In [12] the available volume profiles are all strictly monotonically increasing since the chromosome density was experimentally observed to monotonically decrease away from mid-cell and by definition the profiles are bounded below by zero and above by one. Thus leading to the following clam:

Claim 3: For (20b), suppose that there exists $a_r, b_r, a_m, b_m\in\mathbb{R}$ such that $0 < a_r \leq v_r(x) \leq b_r \leq 1$, $0 < a_m \leq v_m(x) \leq b_m \leq 1$, and $v_r(x), v_m(x)$ are strictly monotonically increasing for $\forall x\in[0,1]$, then:

$$1 < f \leq 1 + \frac{(\frac{b_m}{a_m}-1)(\frac{b_r}{a_r}-1)}{4}.$$

Proof: By Lemma 1, $f > 1$ and by the Grüss inequality [16]:

$$\left|\int_\Omega v_r(x)v_m(x) - \int_\Omega v_r(x)\int_\Omega v_m(x)\right| \leq \tfrac{(b_m-a_m)(b_r-a_r)}{4}$$

$$\implies f - 1 \leq \frac{(b_m-a_m)(b_r-a_r)}{4\int_\Omega v_r(x)\int_\Omega v_m(x)} \leq \frac{(\frac{b_m}{a_m}-1)(\frac{b_r}{a_r}-1)}{4}$$

■

The results of Claim 3 imply that the effective affinity of each mRNA to a ribosome is higher for the fast-diffusion approximation (20) compared to the well-mixed model. For the reminder of this section, we determine the implications of this result on the overall magnitude of $\bar{c}_i$ and how sensitive this quantity is to the activation of a synthetic gene.

We consider the steady state concentrations ($t\to\infty$) of the ODEs in (6) to determine $\bar{c}_i$. We define the total mRNA $\overline{m}_{i,T} = \overline{m}_i + \bar{c}_i$ and total ribosomes $\overline{R}_T = \overline{R} + \sum_{i=1}^N \bar{c}_i$. Thus, from (6):

$$\frac{d\overline{m}_{i,T}}{dt} = \bar{\alpha}_i - (1+\mu)\overline{m}_{i,T}; \quad \frac{d\overline{R}_T}{dt} = \bar{\alpha}_r - \mu\overline{R}_T. \tag{21}$$

The steady states of (21) are: $\overline{m}_{i,T} = \frac{\bar{\alpha}_i}{1+\mu}$ and $\overline{R}_T = \frac{\bar{\alpha}_r}{\mu}$. Denoting the dimensionless dissociation constant as $K_{d,i} =$

$\frac{1+K_i+\mu}{\theta_i}$, the steady state of the ODEs in (6) are given by $\overline{m}_i = \frac{\overline{m}_{i,T}}{1+\overline{R}f_i/K_{d,i}}$ and

$$\bar{c}_i = \frac{\overline{m}_{i,T}\overline{R}f_i/K_{d,i}}{1+\overline{R}f_i/K_{d,i}};\ \overline{R}_T = \overline{R} + \sum_{i=1}^{N} \frac{\overline{m}_{i,T}\overline{R}f_i/K_{d,i}}{1+\overline{R}f_i/K_{d,i}}. \quad (22)$$

Claim 4: Let $\bar{c}_i(f,\overline{R})$ be given explicitly and $\overline{R}(f)$ implicitly by (22), with $f_i = f, \forall i$, where $\overline{m}_{i,T}$, $K_{d,i}$, and $\overline{R}_T$ are fixed parameters. Then, $\bar{c}_i$ and $\overline{R}$ are monotonically increasing and decreasing, respectively, with f.

Proof: We show $\frac{d\bar{c}_i}{df} > 0$ and $\frac{d\overline{R}}{df} < 0$ independent of f. Taking the absolute derivative with respect to f in (22): $\frac{d\overline{R}}{df} = \frac{-\sum_{k=1}^{N}\frac{\partial\bar{c}_k}{\partial f}}{1+\sum_{k=1}^{N}\frac{\partial\bar{c}_k}{\partial\overline{R}}}$, where, $\frac{\partial\bar{c}_k}{\partial f} = \frac{\overline{m}_{k,T}\overline{R}/K_{d,k}}{(1+\overline{R}f/K_{d,k})^2} = \frac{\overline{R}}{f}\frac{\partial\bar{c}_k}{\partial\overline{R}}$, and noting the positivity of $\frac{\partial\bar{c}_k}{\partial f}$ and $\frac{\partial\bar{c}_k}{\partial\overline{R}}$ implies $\frac{d\overline{R}}{df} < 0, \forall f$, as desired. Similarly:

$$\frac{d\bar{c}_i}{df} = \frac{\partial\bar{c}_i}{\partial f} + \frac{\partial\bar{c}_i}{\partial\overline{R}}\frac{d\overline{R}}{df} = \frac{\partial\bar{c}_i}{\partial f}\left(1 - \frac{\frac{f}{\overline{R}}\sum_{k=1}^{N}\frac{\partial\bar{c}_k}{\partial f}}{1+\frac{f}{\overline{R}}\sum_{k=1}^{N}\frac{\partial\bar{c}_k}{\partial f}}\right)$$
$$= \frac{\partial\bar{c}_i}{\partial f}\left(\frac{1}{1+\frac{f}{\overline{R}}\sum_{k=1}^{N}\frac{\partial\bar{c}_k}{\partial f}}\right) > 0, \forall f.$$

■

Claim 3 and Claim 4 imply that the $\bar{c}_i$ predicted by the fast-diffusion approximation is higher than that of the well-mixed model at the expense of $\overline{R}$.

As discussed in Sec. II-C, the input to the system (5) is $\alpha_j(x,t)$ for some j. In terms of concentrations per cell, as in (6), this input at steady state is denoted as $\overline{\alpha}_j = 2\int_\Omega \alpha_j(x, t\to\infty)$. Solutions of the well-mixed model and the fast-diffusion approximation (20), do not depend on the spatial form of $\alpha_j(x,t)$ explicitly, but rather $\overline{\alpha}_j$. From (21), a higher $\overline{\alpha}_j$ increases $\overline{m}_{j,T}$, and from (22), this decreases $\overline{R}$ and $\bar{c}_i, \forall i \neq j$. To quantify how increasing $\overline{\alpha}_j$ decreases $\bar{c}_i, i \neq j$, for the fast-diffusion approximation relative to the well-mixed model, let $f_i = f, \forall i$ and define

$$\Delta_i(\overline{\alpha}_j, f) = \frac{\bar{c}_i(\overline{\alpha}_j, f)}{\bar{c}_i(0,f)},\ \Delta_{i,1}(\overline{\alpha}_j) = \Delta_i(\overline{\alpha}_j, 1), i \neq j. \quad (23)$$

Here, $\Delta_i(\overline{\alpha}_j, f)$ is the normalized sensitivity of $\bar{c}_i$ to $\overline{\alpha}_j$ for a general $f \geq 1$ (as in the fast-diffusion approximation) and $\Delta_{i,1}(\overline{\alpha}_j)$ for the well-mixed model.

Next, we compute (23) using (22) in the special case where $\overline{R}f/K_{d,k} \ll 1, \forall k$ (as assumed in [2]). We are interested in how $\Delta_i(\overline{\alpha}_j, f)$ varies as f increases; however, increasing f may violate the assumption that $\overline{R}f/K_{d,k} \ll 1$. The following claim provides conditions when $\overline{R}f/K_{d,k} \ll 1, \forall k$ may be assumed for all $f \geq 1$.

Claim 5: For $\overline{R}$ given implicitly by (22) where $\overline{m}_{i,T}$, $K_{d,i}$, and $\overline{R}_T$ are fixed parameters and $f_i = f, \forall i$, let $q = \overline{R}f$, $K^+ = \max_k(K_{d,k})$,$K^- = \min_k(K_{d,k})$, and $\phi = \frac{\overline{R}_T}{\sum_{k=1}^{N}\overline{m}_{k,T}}$. Assume $\phi < 1$, then q monotonically increases with f and $K^-\frac{\phi}{1-\phi} \leq q \leq K^+\frac{\phi}{1-\phi}$ as $f \to \infty$.

Proof: To show q is monotonically increasing with f, we show $\frac{dq}{df} > 0$. As in the proof of Claim 4, $\frac{\partial\bar{c}_k}{\partial f} > 0$, thus,

$$\frac{dq}{df} = (R + f\frac{d\overline{R}}{df}) = \left(\frac{\overline{R}}{1+\frac{f}{\overline{R}}\sum_{k=1}^{N}\frac{\partial\bar{c}_k}{\partial f}}\right) > 0,$$

and (22) in terms of q reads: $\overline{R}_T = \frac{q}{f} + \sum_{k=1}^{N}\overline{m}_{k,T}\frac{q/K_{d,k}}{1+q/K_{d,k}}$. Assuming q is bounded above, $\frac{q}{f} \to 0$ as $f \to \infty$. This is true only if $\phi < 1$, since it implies $\overline{R} \to 0$ as $f \to \infty$. Otherwise, if $\phi > 1$, then $R \to \overline{R}_T - \sum_{k=1}^{N}\overline{m}_{k,T}$ as $f \to \infty$. Therefore, as $f \to \infty$, (22) becomes $\overline{R}_T = \sum_{k=1}^{N}\overline{m}_{k,T}\frac{q/K_{d,k}}{1+q/K_{d,k}}$. Notice $\frac{q/K^+}{1+q/K^+} \leq \frac{q/K_{d,k}}{1+q/K_{d,k}} \leq \frac{q/K^-}{1+q/K^-}$, which implies

$$\frac{q/K^+}{1+q/K^+}\sum_{k=1}^{N}\overline{m}_{k,T} \leq \overline{R}_T \leq \frac{q/K^-}{1+q/K^-}\sum_{k=1}^{N}\overline{m}_{k,T}$$

and hence the desired result:

$$K^-\frac{\phi}{1-\phi} \leq q \leq K^+\frac{\phi}{1-\phi}, \quad \text{as } f \to \infty.$$

■

Thus, $K^+\frac{\phi}{1-\phi}$ serves as an upper bound of $\overline{R}f$ for all $f \geq 1$. With this upper bound we can make assumptions that allow us to compare $\Delta_i(\overline{\alpha}_j, f)$ with $\Delta_{i,1}(\overline{\alpha}_j)$ in the special case where $\overline{R}f/K_{d,k} \ll 1, \forall k$ and ensure this assumption is valid even as $f \to \infty$. This is demonstrated below.

Claim 6: For (22), let $K^+ = \max_k(K_{d,k})$,$K^- = \min_k(K_{d,k})$, and $\phi = \frac{\overline{R}_T}{\sum_{k=1}^{N}\overline{m}_{k,T}}$. If $\frac{K^+}{K^-}\frac{\phi}{1-\phi} \ll 1$, then $\Delta_i(\overline{\alpha}_j, f) < \Delta_{i,1}(\overline{\alpha}_j)$ (as in (23)) for $f > 1$ and $\overline{\alpha}_j > 0$.

Proof: By Claim 5, $\frac{K^+}{K^-}\frac{\phi}{1-\phi} \ll 1 \implies \overline{R}f/K_{d,k} \ll 1, \forall k$ regardless of the value of f. Then, from (22), $\Delta_i(\overline{\alpha}_j, f) = \frac{1}{1+\frac{\overline{\alpha}_j/(K_{d,j}(1+\mu))}{1/f+\sum_{k\neq j}\overline{m}_{k,T}/K_{d,k}}}$ which decreases with increasing f. ■

Thus, when $\overline{R}f/K_{d,k} \ll 1, \forall k$, $\bar{c}_i$ is more sensitive to $\overline{\alpha}_j, j \neq i$ for the fast-diffusion approximation than in the well-mixed model.

V. Illustrative Example

In this section, the PDE system (5) is made to illustrate how the activation of a synthetic gene impacts plasmid and chromosome genes. These predictions are both gathered numerically (Sec. VI-B) and compared to the well-mixed model (Def. 1) and the fast-diffusion approximation (20).

A. Parameter Values

For the PDEs in (5), we let: $\alpha_1(x)$ correspond to the lumped endogenous genes, $\alpha_2(x)$ correspond to a plasmid gene with m_2 produced at a constant rate, and $\alpha_3(x)$ correspond to a plasmid gene with m_3 produced at a variable rate. The transcription profile for the endogenous gene $\alpha_1(x) = \alpha_e(x)$ which is defined in Sec. II-B. For the plasmid genes where $i = 2, 3$: $\alpha_i(x) = A_i e^{\frac{-4(1-x)}{l}}$ where $A_i = \frac{2\overline{\alpha}_i}{l(1-e^{\frac{-4}{l}})}$, l is a measure of localization such that $\alpha_i(x) \approx 0, \forall x \in [0, 1-l)$ and A_i was chosen to yield a total production per cell: $2\int_0^1 \alpha_i(x)dx = \overline{\alpha}_i$. The input to (5) is $\alpha_3(x)$, where

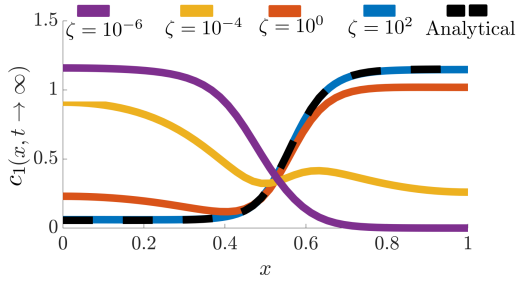

Fig. 2: The spatial steady state profiles of the endogenous mRNA-ribosome complex c_1, for several values of diffusion ζ when $\overline{\alpha}_3 = 0$. Solid lines correspond to the PDE system (5). The dashed line is the fast-diffusion approximation (20), which agrees well with the result for $\zeta = 10^2$. Table I provides the other parameters used.

$\overline{\alpha}_3 \in [0, \overline{\alpha}_e]$. The parameters used in this case study are provided in Sec. VI-A. Using (6), solutions for the well-mixed model are gathered with (7) given by $f_i = 1, \forall i$ and for the fast diffusion approximation, (7) is given by (20b). We define ζ to be a factor that multiplies all diffusion coefficients. If $\zeta = 1$, then the diffusion coefficients are at their nominal values given in Table I.

B. Results

The results of simulating (5) with with the parameters described above are presented here and compared to the fast-diffusion approximation (20) and to the conventional well-mixed ODE model (Definition 1). The steady state spatial profile of the endogenous mRNA-ribosome complex $c_1(x, t \to \infty)$ when $\overline{\alpha}_3 = 0$ (no input) for several values of diffusion (ζ) is shown in Fig. 2 along with the fast-diffusion approximation. For the nominal diffusion level, $\zeta = 1$, the spatial profile is near that of the approximate solution. This agreement improves for $\zeta = 10^2$. For the slow diffusion case $\zeta = 10^{-6}$, the spatial profile is concentrated near mid-cell where most of the endogenous DNA is located. While not shown, $c_2(x, t \to \infty)$ follows a similar trend. For fast diffusion, it converges to the approximate solution and as diffusion slows down, it concentrates near the cell poles where the synthetic DNA is expressed. This spatial separation of mRNAs expressed from plasmids and the chromosome in the limit of slow diffusion, implies that there is minimal cross-talk between plasmid and chromosome genes. This point is illustrated next.

For (5), as $\overline{c}_3$ is expressed (increasing input $\overline{\alpha}_3$), we characterize how this affects $\overline{c}_1$ and $\overline{c}_2$. These results are shown in Fig. 3 for several values of diffusion ζ. The nominal $\zeta = 1$ and fast diffusion $\zeta = 10^2$ cases agree with the well-mixed case. This is expected since for the $v_r(x)$ and $v_m(x)$ used in the simulations, $f = 1.02$ as in (20b). For slow diffusion $\zeta = 10^{-6}$, $\overline{c}_1$ becomes significantly less sensitive to the expression of $\overline{c}_3$ while $\overline{c}_2$ is more sensitive. This is expected since, for slow diffusion, mRNAs localize where they are transcribed: endogenous mRNAs near mid-cell while the plasmid mRNAs in the cell poles.

The available volume profiles $v_r(x)$ and $v_m(x)$, depend on the size and geometry of each species and the chromosome density [12]. Thus, these profiles can vary based

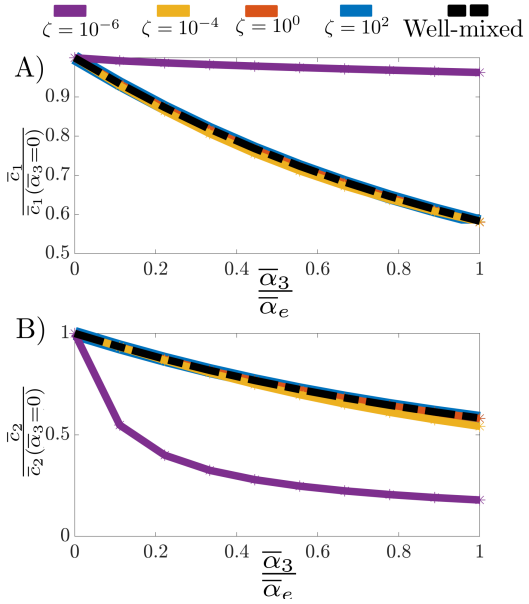

Fig. 3: The protein expression rates per cell (output) as a second plasmid gene is expressed (increasing input $\overline{\alpha}_3$) for several values of diffusion (ζ). The expressions are normalized by the level when $\overline{\alpha}_3 = 0$ (second plasmid gene is silent). $\overline{\alpha}_3$ is normalized by the total endogenous gene mRNA production $\overline{\alpha}_e$. (A) $\overline{c}_1$ and (B) $\overline{c}_2$. Solid lines correspond to the PDE system (5). The dashed line is the well-mixed line ((6) with (7) given by $f_i = 1, \forall i$). Table I provides the other parameters used.

on experimental conditions and compromise the agreement seen in Fig. 3 between the $\zeta = 1$ case and the well-mixed model. To illustrate this, we modify $v_r(x)$ and $v_m(x)$ (as specified in Sec. VI-A) to increase the value of f given by (20b) and evaluate the discrepancies between the PDE (5), well-mixed model, and the fast-diffusion approximation (20). When $\overline{\alpha}_3 = \overline{\alpha}_e$, we define $\Delta_1(f) = \frac{\overline{c}_1(\overline{\alpha}_3, f)}{\overline{c}_1(0, f)}$ and $\Delta_2(f) = \frac{\overline{c}_2(\overline{\alpha}_3, f)}{\overline{c}_2(0, f)}$. In Fig. 4, we show the protein production rate normalized by the well-mixed prediction (A) and Δ_1 and Δ_2 (B) as f varies. These are shown for several values of diffusion, ζ. We observe that the expression of $\overline{c}_1$ and $\overline{c}_2$ increases with f. For $\zeta = 1$, the increase in expression of $\overline{c}_2$ is higher than that of $\overline{c}_1$, but as diffusion increases ($\zeta = 10$) they increase by the same amount. Δ_1 and Δ_2 are more sensitive to $\overline{\alpha}_3$ relative to the well-mixed model as f increases. As diffusion increases (see $\zeta = 10$), the numerical predictions converge to the analytical one. These results are consistent with the theoretical predictions from Sec. IV.

The results from Fig. 4, imply that: even though solutions to (5) can be gathered numerically, depending on the application and system parameters, the ODEs associated with the fast-diffusion approximation (20) can be an alternative. Due to the computational cost, it is advantageous to bypass numerically solving the PDEs in (5).

VI. Conclusions

In this paper, we introduced a ribosome-sharing PDE model that captures the spatial distribution of ribosomes and DNA in the cell, which is not accounted for by common ODE models. The PDE can be used to characterize the

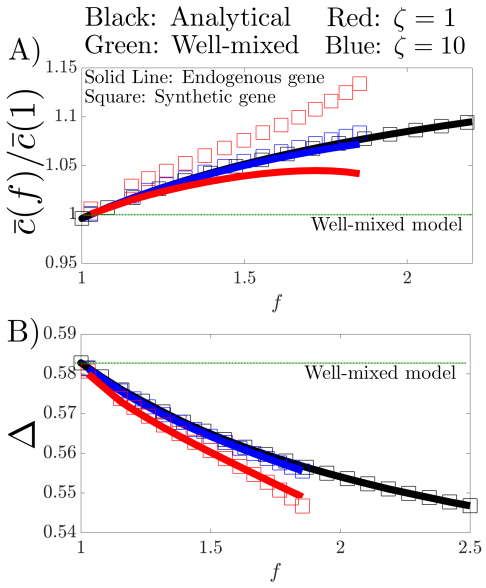

Fig. 4: Numerical simulations of (5). (A) the output $\overline{c}(f)$ when $\overline{\alpha}_3 = 0$ normalized by the well-mixed prediction $\overline{c}(1)$ (Definition 1) (B) The normalized expression Δ when $\frac{\overline{\alpha}_3}{\overline{\alpha}_e} = 1$, as f (given by (20b)) varies. This is shown for $\overline{c}_1$ (solid line) and $\overline{c}_2$ (square) at $\zeta = 1$ (red) and $\zeta = 10$ (blue). The predictions from the fast diffusion approximation model (20) (black line) and the well-mixed model (green) are also shown. Table I provides the other parameters used and Sec. VI-A specifies how $v_r(x)$ and $v_m(x)$ are varied to yield the several values of f.

coupling between genes due to ribosome sharing. Specifically, we investigated the affects of an input signal that activates a synthetic gene on the output expression rate of other genes. The resulting nonlinear PDEs were solved numerically. Through perturbation analysis, we showed that in the limit of fast diffusion that mRNA and ribosome spatial profiles are not homogeneous. The profiles mirror the available volume profiles and their monotonicity implies that all mRNAs in the cell have a higher affinity to bind to ribosomes relative to the standard "well-mixed" ODE model. This increased affinity implies higher protein production rate for all mRNAs in the cell, and in some cases, the production rate is more sensitive to the activation of a synthetic gene. These results were observed numerically for the full PDE system using known biological parameters found in the literature. With these parameters, the well-mixed ODE model and PDE model matched well. We provided an example where these two models do not agree, however, the fast-diffusion approximation was a better alternative to the well-mixed model. This approximation bypasses having to solve the PDEs and thus saves computational effort. In future work, we wish to prove the stability of the steady state solutions, derive higher order correction factors to the perturbation expansion, and account for changes in growth rate as synthetic genes are expressed.

ACKNOWLEDGMENT

We thank Yili Qian and Cameron McBride for proofreading the manuscript. We thank the National Science Foundation Graduate Research Fellowship and the Ford Foundation Fellowship programs for their funding.

Parameter	Value	Ref.	Parameter	Value	Ref.
μ	0.1	[2]	θ_i	125	[6]
K_i	10	[2],[12]	l	0.5	
$\overline{\alpha}_r$	$3/4\frac{\mu}{1+\mu}$	[12],[22]	χ	9.4	[12]
$\overline{\alpha}_1$	$1/41.4$	[23],[24],[17]	χ_r	8χ	[12]

TABLE I: The dimensionless parameters used in this study.

APPENDIX

A. Parameters

We model the volume profiles as in [12], which are empirically derived from experimental data. The ribosome available volume profile is $v_r(x) = e^{-0.188\rho(x)}$, for free mRNA $v_m(x) = e^{-.754\rho(x)}$, for the mRNA-ribosome complex we used the available volume profile that corresponds to a complex with the average number of ribosomes (12) such that $v_c(x) = e^{-3.01\rho(x)}$. Recalling the endogenous mRNA production rate $\alpha_{e,l}$, the cell length L, and the mRNA degradation rate γ were used to nondimensionlize the governing equations. Again, the parameters provided below will be dimensionless.

Typical growth (dilution) rates of the cell can be as high as 2 hr^{-1} (20 minute doubling time) and as low as 0.1 hr^{-1} (416 minute doubling time) [25] depending on the strain phenotype and growth conditions (e.g., media and temperature). mRNA half lives are typically 3-8 min (5-14 hr^{-1}) [6]. In this example we chose $\mu = 0.1$ (dilution is a tenth of mRNA degradation) consistent with a healthy growing cell. In [12] $\kappa_i + d_i = 10\gamma$, hence $K_i = \frac{\kappa_i + d_i}{\gamma} = 10$ for all species.

The number of endogenous mRNA per cell is 5×10^3 [12]. For a cell doubling time of 30 minutes, the number of ribosomes per cell is 45×10^3 [22]. On average, 12 ribosomes load a single mRNA, hence $\overline{\alpha}_r = N_{\text{ribo}}/(12N_{\text{mRNA}}) = \overline{\alpha}_r \frac{\mu}{1+\mu} = 3/4\frac{\mu}{1+\mu}$.

The total endogenous mRNA concentration is 4140 mRNAs per cell and the synthetic mRNA concentration can vary between $0-1000$ mRNA's per cell depending on the plasmid copy number [23]. We assume that m_1 is expressed from a medium copy plasmid and hence $\overline{\alpha}_2 = 100/4140$ and allow $\overline{\alpha}_3$ to vary.

In [6] it was shown 80% of ribosomes were translating an mRNA, hence we chose θ_i (same for all species) such that with the given number of total ribosomes and endogenous mRNA: $\frac{\overline{c}_e}{\overline{R}_T} = 0.8$ in isolation (no synthetic genes). This corresponds to $\theta_i = 125$.

The measure of localization l was set at $l = 0.5$. For $L = 1.5$ μm, $D_m = 0.05$ μm^2/s, and $\gamma = 10$ h^{-1} as in [12], $\chi_m = 9.4$. The ribosomal diffusion is $\chi_r = 8\chi_m$ [12].

In Sec. V-B, to generate the results in Fig. 4, we allowed f as defined by (20b) to vary. Variations in f were accomplished by:

$$f(n) = \frac{\int_0^1 \left[v_r(x)\right]^{4n}\left[v_m(x)\right]^n dx}{\int_0^1 \left[v_r(x)\right]^{4n} dx \int_0^1 \left[v_m(x)\right]^n dx},$$

for $n \in (1, 4]$.

B. Numerical Collocation Method

This section introduces the numerical method used to numerically simulate (5). We make use of the notation introduced in Sec. III. Let $\boldsymbol{y} = [R, m_1, \ldots, m_N, c_1, \ldots, c_N]^T$ be the species corresponding to the system (5) and $M = 2N+1$. For each species $\boldsymbol{y}^j(x,t)$ with an available volume profile $v_j(x)$, consider the change of variables: $\boldsymbol{w}^j(x,t) = \frac{\boldsymbol{y}^j(x,t)}{v_j(x)}$. This change of variables renders a simpler set of boundary conditions (homogeneous Neumann):

$$\left.\frac{\partial \boldsymbol{w}(x,t)}{\partial x}\right|_{x=0,1} = 0.$$

Compactly expressing (5a)-(5c) after the change of coordinates as:

$$\frac{\partial \boldsymbol{w}}{\partial t} = \boldsymbol{f}(\boldsymbol{w}, \boldsymbol{w}_x, \boldsymbol{w}_{xx}, x, t), \tag{24}$$

where $\boldsymbol{f} : D \times [0,1] \times [t_0, t_1] \to \mathbb{R}^M$, $0 \leq t_0 < t_1$, $D \subset \mathbb{R}^M$ and subscripts of x denote partial differentiation with respect to x. A set of initial conditions are prescribed to uniquely define the problem.

A collocation method is implemented to numerically solve (24) . We expand $\boldsymbol{w}^j(x,t)$ by a set of orthonormal basis $\{\phi_i(x)\}$ of $L^2([0,1])$:

$$\boldsymbol{w}^j(x,t) = \sum_{i=0}^{\infty} a_{ji}(t)\phi_i(x), \tag{25}$$

where $a_{ji}(t) \in \mathbb{R}$ is the weight of the projection of $\boldsymbol{w}^j(x,t)$ onto $\phi_i(x)$. An admissible basis (satisfies the boundary conditions) is $\phi_i(x) = \cos(i\pi x)$. A general Fourier series expansion for $\boldsymbol{w}^j(x,t)$ was possible, however all the sine terms would nullify to satisfy the "flux" free boundary conditions, resulting in the current expansion.

Let $\boldsymbol{w}_n^j(x,t) = \sum_{i=0}^{n} a_{ji}(t)\cos(i\pi x)$ be the truncated expansion of $\boldsymbol{w}^j$. This approximate solution will not satisfy (24), instead:

$$\frac{\partial \boldsymbol{w}_n^j}{\partial t} = \boldsymbol{f}^j(\boldsymbol{w}_n, \boldsymbol{w}_{n,x}, \boldsymbol{w}_{n,xx}, x, t) + \epsilon_j(x,t), \tag{26}$$

where $\epsilon_j(x,t) \in \mathbb{R}$ denotes the error term (residual) arising from the approximation. The collocation method requires the error to vanish at $x = x_i (i = 0, 1, \ldots, n)$, the collocation points. As a consequence:

$$\frac{\partial \boldsymbol{w}_n^j(x_i,t)}{\partial t} = f_j(\boldsymbol{w}_n(x_i,t), \boldsymbol{w}_{n,x}(x_i,t), \boldsymbol{w}_{n,xx}(x_i,t), x_i, t), \tag{27}$$

for each $i = 0, 1 \ldots, n$. This yields a system of $M \times (n+1)$ ordinary differential equations for each $a_{ji}(t)$.

REFERENCES

[1] D. Del Vecchio, A. J. Dy, and Y. Qian, "Control theory meets synthetic biology," *J. R. Soc. Interface*, vol. 13, no. 120, p. 20160380, 2016.

[2] A. Gyorgy, J. I. Jiménez, J. Yazbek, H. H. Huang, H. Chung, R. Weiss, and D. Del Vecchio, "Isocost Lines Describe the Cellular Economy of Genetic Circuits," *Biophys. J.*, vol. 109, no. 3, pp. 639–646, 2015.

[3] I. Shachrai, A. Zaslaver, U. Alon, and E. Dekel, "Cost of Unneeded Proteins in E. coli Is Reduced after Several Generations in Exponential Growth," *Mol. Cell*, vol. 38, no. 5, pp. 758–767, 2010.

[4] Y. Qian, H. H. Huang, J. I. Jiménez, and D. Del Vecchio, "Resource Competition Shapes the Response of Genetic Circuits," *ACS Synth. Biol.*, vol. 6, no. 7, pp. 1263–1272, 2017.

[5] Y. Qian and D. Del Vecchio, "Mitigation of ribosome competition through distributed sRNA feedback," *2016 IEEE 55th Conf. Decis. Control. CDC 2016*, pp. 758–763, 2016.

[6] S. Bakshi, A. Siryaporn, M. Goulian, and J. C. Weisshaar, "Superresolution imaging of ribosomes and RNA polymerase in live Escherichia coli cells," *Mol. Microbiol.*, vol. 85, no. 1, pp. 21–38, 2012.

[7] S. Yao, D. R. Helinski, and A. Toukdarian, "Localization of the naturally occurring plasmid ColE1 at the cell pole," *J. Bacteriol.*, vol. 189, no. 5, pp. 1946–1953, 2007.

[8] A. Amir and S. van Teeffelen, "Getting into shape: How do rod-like bacteria control their geometry?," *Syst. Synth. Biol.*, vol. 8, no. 3, pp. 227–235, 2014.

[9] Leah Edelstein-Keshet, "Mathematical Models in Biology," *Siam*, vol. XXXIII, no. 2, pp. 81–87, 2012.

[10] R. J. Brooker, E. P. Widmaier, L. E. Graham and P. Stilling, "Biology," McGraw-Hill, New York, 2014.

[11] D. Del Vecchio and R. M. Murray, "Biomolecular feedback systems," Princeton: Princeton University Press, 2014.

[12] M. Castellana, S. Hsin-Jung Li, and N. S. Wingreen, "Spatial organization of bacterial transcription and translation," *Proc. Natl. Acad. Sci.*, vol. 113, no. 33, pp. 9286–9291, 2016.

[13] J. Salje, "Plasmid segregation: how to survive as an extra piece of DNA," *Crit. Rev. Biochem. Mol. Biol.*, vol. 45, no. 4, pp. 296–317, 2010.

[14] W. Chen, M. Niepel, and P. Sorger, "Classic and contemporary approaches to modeling biochemical reactions," *Genes Dev.*, vol. 24, pp. 1861–1875, 2010.

[15] S. H. Cho, J. M. Godin, C.-H. Chen, W. Qiao, H. Lee, and Y.-H. Lo, "Review Article: Recent advancements in optofluidic flow cytometer," *Biomicrofluidics*, vol. 4, p. 043001, dec 2010.

[16] D. S. Mitrinović, J. E. Pečarić, and A. M. Fink, *Classical and New Inequalities in Analysis*. Dordrecht: Springer Netherlands, 1993.

[17] U. Alon, "An Introduction to Systems Biology: Design Principles of Biological Circuits," 2007.

[18] M. H. Holmes, "Introduction to Perturbation Methods - Matched Asymptotic Epansions," in *ZAMM - J. Appl. Math. Mech. / Zeitschrift für Angew. Math. und Mech.*, vol. 76, pp. 384–384, 1996.

[19] L. V. Kalachev, H. G. Kaper, and T. J. Kaper, "Reduction for michaelis-menten-henri kinetics in the presence of diffusion," pp. 155–184, 2007.

[20] M. Renardy and R. C. Rogers, "An Introduction to Partial Differential Equations," *Differ. Equations*, vol. 13, no. 2, pp. 1–5, 2003.

[21] H. L. Smith, *Monotone Dynamical Systems: An Introduction to the Theory of Competitive and Cooperative Systems*, vol. 41. 1995.

[22] F. Neidhardt, *Escherichia coli and Salmonella: Cellular and Molecular Biology*. 1996.

[23] T. E. Gorochowski, I. Avcilar-Kucukgoze, R. A. Bovenberg, J. A. Roubos, and Z. Ignatova, "A Minimal Model of Ribosome Allocation Dynamics Captures Trade-offs in Expression between Endogenous and Synthetic Genes," *ACS Synth. Biol.*, vol. 5, no. 7, pp. 710–720, 2016.

[24] J. Norrander, T. Kempe, and J. Messing, "Construction of improved M13 vectors using oligodeoxynucleotide-directed mutagenesis," *Gene*, vol. 26, no. 1, pp. 101–106, 1983.

[25] F. Ceroni, R. Algar, G.-B. Stan, and T. Ellis, "Quantifying cellular capacity identifies gene expression designs with reduced burden," *Nat. Methods*, vol. 12, no. 5, pp. 415–418, 2015.